

THREE-LAYER FLUID FLOW OVER A SMALL OBSTRUCTION ON THE BOTTOM OF A CHANNEL

SRIKUMAR PANDA¹, S. C. MARTHA ¹ and A. CHAKRABARTI²

(Received 5 December, 2013; revised 21 July, 2014; first published online 20 January 2015)

Abstract

Many boundary value problems occur in a natural way while studying fluid flow problems in a channel. The solutions of two such boundary value problems are obtained and analysed in the context of flow problems involving three layers of fluids of different constant densities in a channel, associated with an impermeable bottom that has a small undulation. The top surface of the channel is either bounded by a rigid lid or free to the atmosphere. The fluid in each layer is assumed to be inviscid and incompressible, and the flow is irrotational and two-dimensional. Only waves that are stationary with respect to the bottom profile are considered in this paper. The effect of surface tension is neglected. In the process of obtaining solutions for both the problems, regular perturbation analysis along with a Fourier transform technique is employed to derive the first-order corrections of some important physical quantities. Two types of bottom topography, such as concave and convex, are considered to derive the profiles of the interfaces. We observe that the profiles are oscillatory in nature, representing waves of variable amplitude with distinct wave numbers propagating downstream and with no wave upstream. The observations are presented in tabular and graphical forms.

2010 *Mathematics subject classification*: primary 35Q35; secondary 76B07.

Keywords and phrases: linear theory, three-layer irrotational flow, perturbation analysis, Fourier transformation, concave and convex bottom profiles.

1. Introduction

Recently, researchers have faced various challenges in modelling free-surface fluid flow over submerged obstacles. In general, flow over a submerged obstacle is studied in engineering, atmospheric and oceanographic sciences. One such important study is the free-surface fluid flow over different kinds of obstacles at the bottom of a channel. Based on an extensive literature survey, we have observed that a major thrust area of research is to model free-surface flows over different kinds of obstacles situated at the

¹Department of Mathematics, Indian Institute of Technology Ropar, Rupnagar 140001, Punjab, India; e-mail: srikumarp@iitrpr.ac.in, scmartha@iitrpr.ac.in.

²Department of Mathematics, Indian Institute of Science, Bangalore 560012, India; e-mail: aloknath.chakrabarti@gmail.com.

© Australian Mathematical Society 2015, Serial-fee code 1446-1811/2015 \$16.00

bottom of an infinite channel. For instance, Lord Kelvin [23] studied the flow in a channel having a bottom obstruction that resembles ridges and hollows using linear theory, and Lamb [21] used linear theory to calculate the drag force on a cylindrical obstruction attached to the bottom. Long [22] linearized the governing equations around the uniform upstream flow and obtained solutions representing waves.

On the other hand, attention to nonlinear free-surface flow over an irregular bottom has rapidly increased over the last three decades. Substantial progress has been made in this direction by many researchers. Forbes and Schwartz [17] considered the flow over a semicircular obstruction and calculated the wave resistance offered by the semicircle, by utilizing a numerical approach to the associated flow problem. Vanden-Broeck [28] numerically solved the same problem considered by Forbes and Schwartz [17], and discussed the existence of supercritical solutions dependent on the Froude number. Later, Forbes [13] presented a numerical solution for critical free-surface flow over a semicircular obstruction attached to the bottom of a running stream. Yong [31] used perturbation as well as numerical methods to study the generation of nonlinear capillary-gravity waves in a fluid system having a concave bottom including the effect of surface tension. Dias and Vanden-Broeck [8] studied the problem involving free-surface flow past a submerged triangular obstacle at the bottom of a channel, and solved the problem numerically by series truncation. Shen et al. [25] obtained the numerical solution for the steady surface waves on an incompressible and inviscid fluid flow over a semicircular as well as a semielliptical obstacle at the bottom. Dias and Vanden-Broeck [10] solved the steady free-surface flow problem numerically, and demonstrated that there are supercritical flows with waves existing only downstream. Higgins et al. [19] presented an analytical series method to obtain the solution of the problem involving flow over topography. They calculated the analytical series solutions for supercritical, transcritical and subcritical flow regimes over the considered topography. The above studies were focused on the solution of the problem involving a steady flow only. For the problems involving unsteady flow, Grimshaw and Smyth [18] presented a theoretical study of a stratified fluid flow over bottom topography. They solved the problem using weak nonlinear theory and pointed out that the flow can be described by a forced Korteweg–de Vries (KdV) equation. Stokes et al. [26] used a numerical technique to analyse the unsteady flow with a submerged point sink beneath the free surface. Milewski and Vanden-Broeck [24] considered the time-dependent free-surface flow over a submerged moving obstacle on a shallow water channel and solved the problem using weak nonlinear theory. All the above studies were carried out by assuming fluid flow in a single layer.

Following this, flow problems in a single layer have been extended to two layers of fluids. In 1989, Forbes [14] developed a numerical solution of a two-layer critical flow problem over a semicircular obstruction attached to the bottom. He solved the problem with the help of conformal mapping along with an integro-differential equation approach. Belward and Forbes [2] considered the steady flow in a two-layer fluid where the upper fluid layer is bounded by a rigid lid. They have presented the solution of the problem using linear as well as nonlinear theory. They have shown that

the interface profile is oscillatory in nature, representing a wave of constant amplitude with one wave number. Dongqiang et al. [11] described the Hamiltonian canonical equations for nonlinear waves in a two-layer fluid with a horizontal bottom. The flow problem in two layers has also been studied by Chakrabarti and Martha [6] using linear as well as weakly nonlinear theory. Dias and Vanden-Broeck [9] considered nonlinear waves in a forced channel flow over a bottom obstacle. They obtained a numerical solution with the help of a boundary integral equation technique. Note that the two-layer fluid flow problem discussed above can be reduced to a single-layer fluid flow problem by considering the upper layer to have zero density.

Based on an extensive survey of literature of free-surface flow over an obstacle at the bottom of a channel, it has been observed that study of three-layer fluid flow over arbitrary bottom topography is scarce. Such study is important in considering the problem of flow in an oceanographic or a meteorological situation, since the single- or the two-layer approximation becomes insufficient due to the continuous stratification of the fluid, as pointed out by Belward and Forbes [2]. Therefore, the next step is to undertake a comprehensive modelling effort for fluid flow in three layers that may lead to a better understanding of the atmospheric situations. Thus, the present paper considers two linearized flow problems involving three-layer fluid over an irregular bottom topography having a small undulation. The two linearized flow problems are:

- (a) flow in a three-layer fluid when the uppermost layer is bounded by a rigid lid; and
- (b) flow in a three-layer fluid when the uppermost layer is free to the atmosphere.

In general, the rigid-lid approximation is used by many researchers (see, for example, [2, 6, 12]) to simplify their models. In a rigid-lid approximation, the free-surface displacements compared to the interface displacements are neglected. However, in case of a flow with a free surface, the free-surface displacements cannot be neglected. The aim of the present study is to demonstrate the behaviour of the interface profiles for both cases. The fluids in each layer are assumed to be immiscible, inviscid and incompressible. Moreover, the density of the fluid in each layer is considered to be different. This work is an extension of the work of Belward and Forbes [2], where the problem of two-layer fluid flow was handled in the light of both linear as well as nonlinear theory. Note that the three-layer fluid flow problem resembles a physical situation of flow in a channel, where the uppermost layer of the three-layer fluid is that of fresh water, the middle layer is of salty water and the bottommost layer is of muddy water. This situation can be visualized while understanding the circulation generated beneath melting ice sheets, and the subsequent interaction of fresh and salt water gives rise to a type of intrusive current as noticed by Williams et al. [29]. The flow problem involving three-layer fluid is also important, since it appears in some practical situations as pointed out by Forbes et al. [7, 15, 16]. It may be emphasized that, in practice, one may encounter flow problems involving multiple layers of fluids of different densities. Therefore, generalizing the problem involving a two-layer fluid to that involving a three-layer fluid, considered in the present work, is

an endeavour to take the matters to another step forward towards a real and practical situation occurring in channel flow problems. In addition, this paper also highlights the role of the Fourier transform method for a more general problem like the three-layer flow problem in an elaborate way, as compared to the two-layer flow problem studied by earlier researchers.

Using linear theory and with the assumption of irrotational motion, each flow problem is formulated as three boundary value problems (BVPs). The BVPs comprise three potential functions describing the fluid motion in each layer. Perturbation analysis involving a small parameter ε (height of the obstacle) is employed in the governing equations and therefore the original BVPs are reduced to simpler BVPs in order to determine the first-order velocity potentials as well as the interface profiles. Fourier transformation is used to derive the analytical expressions of the velocity potentials and interface profiles. These profiles are obtained in terms of integrals. We observe that these integrals depend on the bottom profile. In order to study the influence of natural and individual variation of the bottom profile on the essence of interface profiles, two different kinds of bottom profiles, such as concave and convex, are considered in both the problems separately. In this study, the nature of the roots of the dispersion relation, which is an important relation of the study involving fluid flow, associated with both the flow problems, is investigated in detail with the help of Rouché's theorem [27]. The numerical results are tabulated and illustrated in graphical forms to understand the effect of some important physical quantities on the behaviour of interfaces. We also observe that the interfacial profiles are oscillatory in nature, representing waves of variable amplitude with different wave numbers which lead to several interesting features, such as wavy solutions giving rise to a wave-free solution for certain parameter values, beating-like behaviour, downstream resonances and so on. These phenomena are noticed in our study, which are not reported in earlier works. In addition, it has been observed that the interface profiles exhibit a wave-free region upstream of the obstacle followed by a wavy region downstream of the obstacle.

After describing the problems under consideration in Section 2, the formulation and the solution procedure corresponding to the case of a bounded uppermost layer and that for the case of a free surface are detailed in Sections 3 and 4, respectively. In Section 5, the numerical results are discussed and, in Section 6, the overall study is summarized.

2. Description of the problems

We consider a system composed of three layers of fluids flowing in an infinite channel having an irregular bottom. It is assumed that the fluid in each layer is inviscid, incompressible and immiscible, and has varying density. The effect of surface tension is ignored. It is further assumed that the flow in each layer is two dimensional and irrotational with uniform velocity far upstream. The profile of the irregular bottom topography is given by $y = B(x)$, where the x -axis is chosen to be along the bottom of the channel and the y -axis is measured vertically upward. Moreover, the study

comprises two flow problems involving three-layer fluid: (a) when the uppermost fluid layer is bounded by a rigid lid and (b) when it is free to the atmosphere. We denote the upstream depths, upstream horizontal velocities, densities, velocities and pressures by H_j , c_j , ρ_j , \vec{q}_j and p_j , respectively, for $j = 1, 2, 3$. Note that subscripts 1, 2 and 3 refer to quantities in the lowest, middle and uppermost layers, respectively. The interface between the lower layer and the middle layer is represented by $y = S(x)$ and the interface between the middle layer and the uppermost layer is represented by $y = Q(x)$. These interface profiles are unknown at the outset. The free surface is represented by $y = P(x)$. Let ϕ_j ($j = 1, 2, 3$) be the velocity potential in layer j . So, $\vec{q}_j = (u_j, v_j) = (\phi_{j,x}, \phi_{j,y})$, where $\phi_{j,x}$ and $\phi_{j,y}$ denote the partial derivatives of ϕ_j with respect to x and y , respectively. The entire flow system is subjected to the downward acceleration due to gravity, g . In this study, we have only considered the waves that are stationary with respect to the bottom profile and, hence, the partial derivatives with respect to time are equal to zero.

The problems under consideration are nondimensionalized by using H_1 as the length scale and c_1 as the velocity scale. As a result, the bottommost layer has an upstream uniform speed and a height of unity. We have introduced seven dimensionless quantities

$$\begin{aligned} \lambda_1 &= H_3/H_1, & \lambda_2 &= H_2/H_1 & & \text{(ratio of upstream depths of fluids),} \\ D_1 &= \rho_3/\rho_2, & D_2 &= \rho_2/\rho_1 & & \text{(ratio of densities),} \\ \gamma_1 &= c_3/c_1, & \gamma_2 &= c_2/c_1 & & \text{(ratio of upstream fluid speeds),} \\ F &= c_1/\sqrt{gH_1} & & & & \text{(Froude number),} \end{aligned}$$

which describe the properties of the flow, and two dimensionless parameters, ε (obstacle height) and L (obstacle half-length), which describe the properties of the obstacle. Therefore, the work proceeds purely with nondimensional variables.

3. Three-layer flow when the uppermost layer is bounded by a rigid lid

In this section, we consider the fluid flow problem involving three layers of fluids in an infinite channel associated with an irregular bottom having a small undulation. The uppermost fluid layer is bounded by a rigid lid. The fluid system is shown schematically in Figure 1.

3.1. Mathematical formulation The flow problem considered in this section gives rise to the following BVPs for the determination of the velocity potential $\phi_j(x, y)$ in each layer. Within each layer, the equation of continuity yields

$$\nabla^2 \phi_j = 0 \quad \text{for } j = 1, 2, 3, \quad (3.1)$$

where ∇^2 is the two-dimensional Laplacian operator.

As there is no incursion, the condition on the upper boundary of the uppermost layer is written as

$$\phi_{3,y} = 0 \quad \text{on } y = 1 + \lambda_1 + \lambda_2. \quad (3.2)$$

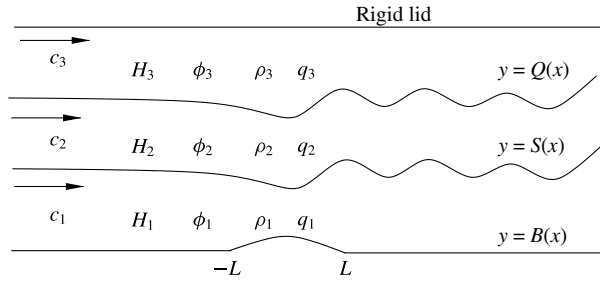


FIGURE 1. Definition sketch of three-layer fluid flow when the uppermost layer is bounded by a rigid lid.

At each interface, there is no fluid exchange and, hence, the conditions at the interfaces are

$$\phi_{j,n} = 0 \quad \text{for } j = 1, 2 \quad \text{on } y = S(x), \tag{3.3}$$

$$\phi_{j,n} = 0 \quad \text{for } j = 2, 3 \quad \text{on } y = Q(x), \tag{3.4}$$

where $\partial/\partial n$ is the normal derivative at a point (x, y) at the respective surfaces.

As there is no incursion at the bottom, the bottom boundary condition may be written as

$$\phi_{1,n} = 0 \quad \text{on } y = B(x). \tag{3.5}$$

The continuity of pressure coupled with Bernoulli's equation [1] gives rise to the matching conditions for the interfaces, and these are expressed as

$$\frac{F^2}{2}(q_1^2 - D_2 q_2^2) + (1 - D_2)S(x) = \frac{F^2}{2}(1 - D_2 \gamma_2^2) + (1 - D_2) \quad \text{on } y = S(x), \tag{3.6}$$

$$\frac{F^2}{2}(q_2^2 - D_1 q_3^2) + (1 - D_1)Q(x) = \frac{F^2}{2}(\gamma_2^2 - D_1 \gamma_1^2) + (1 + \lambda_2)(1 - D_1) \quad \text{on } y = Q(x). \tag{3.7}$$

In addition to the conditions (3.1)–(3.7), there are conditions far upstream, and these are

$$\begin{aligned} \vec{q}_1 &\rightarrow \vec{i}, & \vec{q}_2 &\rightarrow \gamma_2 \vec{i}, & \vec{q}_3 &\rightarrow \gamma_1 \vec{i}, & S(x) &\rightarrow 1, \\ Q(x) &\rightarrow 1 + \lambda_2 \quad \text{as } x \rightarrow -\infty. \end{aligned} \tag{3.8}$$

Our objective is to determine the unknown functions ϕ_j ($j = 1, 2, 3$), $S(x)$ and $Q(x)$. These unknowns can be determined once the BVPs involving relations (3.1)–(3.8) are solved completely. In the following section, the above BVPs are solved with the help of perturbation analysis along with a Fourier transform technique.

3.2. Method of solution and results We assume that the bottom profile is given by $B(x) = \varepsilon f(x)$, where ε , a dimensionless small quantity, is the height of the bottom

profile. According to the conditions in (3.8), the velocity potentials and the interface profiles can be expressed in terms of the perturbation parameter ε as follows:

$$\phi_3(x, y) = \gamma_1 x + \varepsilon \phi_{31}(x, y) + O(\varepsilon^2), \tag{3.9}$$

$$\phi_2(x, y) = \gamma_2 x + \varepsilon \phi_{21}(x, y) + O(\varepsilon^2), \tag{3.10}$$

$$\phi_1(x, y) = x + \varepsilon \phi_{11}(x, y) + O(\varepsilon^2), \tag{3.11}$$

$$S(x) = 1 + \varepsilon S_1(x) + O(\varepsilon^2), \tag{3.12}$$

$$Q(x) = 1 + \lambda_2 + \varepsilon Q_1(x) + O(\varepsilon^2), \tag{3.13}$$

where ϕ_{j1} ($j = 1, 2, 3$), $S_1(x)$ and $Q_1(x)$ denote the first-order corrections of velocity potential ϕ_j , $S(x)$ and $Q(x)$, respectively.

In order to determine the velocity potentials ϕ_j ($j = 1, 2, 3$) and the profiles $S(x)$ and $Q(x)$, the first-order corrections ϕ_{31} , ϕ_{21} , ϕ_{11} , $S_1(x)$ and $Q_1(x)$ have to be evaluated. Now, substituting the relations (3.9)–(3.13) in relations (3.1)–(3.7), we have obtained the following BVPs for the order of ε^1 :

$$\begin{aligned} \nabla^2(\phi_{11}, \phi_{21}, \phi_{31}) &= 0 \quad (\text{within each layer}), \\ \phi_{31,y} &= 0 \quad \text{on } y = 1 + \lambda_1 + \lambda_2, \\ \phi_{31,y} &= \gamma_1 Q'_1(x) \quad \text{on } y = 1 + \lambda_2, \\ \phi_{21,y} &= \gamma_2 Q'_1(x) \quad \text{on } y = 1 + \lambda_2, \\ \phi_{21,y} &= \gamma_2 S'_1(x) \quad \text{on } y = 1, \\ \phi_{11,y} &= S'_1(x) \quad \text{on } y = 1, \\ \phi_{11,y} &= f'(x) \quad \text{on } y = 0, \\ F^2(\phi_{11,x} - D_2 \gamma_2 \phi_{21,x}) + (1 - D_2)S_1(x) &= 0 \quad \text{on } y = 1, \\ F^2(\gamma_2 \phi_{21,x} - D_1 \gamma_1 \phi_{31,x}) + (1 - D_1)Q_1(x) &= 0 \quad \text{on } y = 1 + \lambda_2, \end{aligned} \tag{3.14}$$

where the symbol ' denotes the first-order derivative.

In order to solve the BVPs given by (3.14), we assume that the Fourier transforms of the first-order velocity potentials $\phi_{j1}(x, y)$ ($j = 1, 2, 3$) and the bottom profile $f(x)$ exist, and are defined as

$$\widehat{\phi}_{j1}(k, y) = \int_0^\infty \phi_{j1}(x, y) \sin(kx) dx \quad (j = 1, 2, 3),$$

with inverse transform

$$\phi_{j1}(x, y) = \frac{2}{\pi} \int_0^\infty \widehat{\phi}_{j1}(k, y) \sin(kx) dk \quad (j = 1, 2, 3),$$

and

$$f(x) = \int_0^\infty M(k) \cos(kx) dk, \tag{3.15}$$

where $M(k)$ determines the bottom profile. Similarly, the transforms of $S_1(x)$ and $Q_1(x)$ are defined as

$$S_1(x) = \int_0^\infty a(k) \cos(kx) dk \quad \text{and} \quad Q_1(x) = \int_0^\infty b(k) \cos(kx) dk. \tag{3.16}$$

By applying these transforms to the BVPs given by (3.14) and solving them, we obtain the first-order potentials

$$\begin{aligned}\phi_{31}(x, y) &= \int_0^\infty \frac{\gamma_1 b(k)}{\sinh(k\lambda_1)} \cosh k(y-1-\lambda_1-\lambda_2) \sin(kx) dk, \\ \phi_{21}(x, y) &= \int_0^\infty \left\{ \frac{\gamma_2 [a(k) - b(k) \cosh(k\lambda_2)]}{\sinh(k\lambda_2)} \cosh k(y-1-\lambda_2) \right. \\ &\quad \left. - \gamma_2 b(k) \sinh k(y-1-\lambda_2) \right\} \sin(kx) dk\end{aligned}$$

and

$$\phi_{11}(x, y) = \int_0^\infty \left[\frac{M(k) - a(k) \cosh k}{\sinh k} \cosh k(y-1) - a(k) \sinh k(y-1) \right] \sin(kx) dk,$$

where

$$a(k) = \frac{F^2 k M(k) E_4(k) \sinh(k\lambda_2)}{E_5(k)} \quad \text{and} \quad b(k) = \frac{F^2 \gamma_2^2 k a(k) \sinh(k\lambda_1)}{E_4(k)}, \quad (3.17)$$

with

$$\begin{aligned}E_4(k) &= F^2 \gamma_2^2 k \cosh(k\lambda_2) \sinh(k\lambda_1) + F^2 \gamma_1^2 k D_1 \cosh(k\lambda_1) \sinh(k\lambda_2) \\ &\quad - (1 - D_1) \sinh(k\lambda_1) \sinh(k\lambda_2), \\ E_5(k) &= E_4(k) \{ F^2 k \cosh k \sinh(k\lambda_2) + [\gamma_2^2 F^2 k D_2 \cosh(k\lambda_2) \\ &\quad - (1 - D_2) \sinh(k\lambda_2)] \sinh k \} - \gamma_2^4 F^4 k^2 D_2 \sinh k \sinh(k\lambda_1).\end{aligned}$$

The first-order interface profiles, $S_1(x)$ and $Q_1(x)$, are obtained in terms of integrals as in (3.16). Further, the first-order interface profiles depend on the bottom profile (refer to equations (3.15) and (3.17)). The resulting integrals can be evaluated when $f(x)$ is known. In the following section, we consider special forms for the function $f(x)$.

3.3. Special forms of the bottom profiles In order to demonstrate the influence of natural and individual variation of bottom topography on the behaviour of interface profiles, the study is performed by considering two different kinds of bottom profiles, one of which is concave and the other convex. The bottom profiles considered in this section are intended to correspond to the bumped shapes encountered in practical situations.

EXAMPLE 3.1 (Concave bottom profile). Let us consider a smooth concave bottom profile given by

$$f(x) = \begin{cases} \frac{1}{2} \left(1 + \cos \frac{\pi x}{L} \right) & \text{if } -L \leq x \leq L, \\ 0 & \text{otherwise.} \end{cases}$$

In this context, relations (3.15) and (3.17) yield

$$a(k) = \frac{F^2 \pi \sin(kL) E_4(k) \sinh(k\lambda_2)}{(\pi^2 - k^2 L^2) E_5(k)} \quad \text{and} \quad b(k) = \frac{F^4 \gamma_2^2 \pi k \sin(kL) \sinh(k\lambda_1) \sinh(k\lambda_2)}{(\pi^2 - k^2 L^2) E_5(k)}.$$

By substituting $a(k)$ and $b(k)$ in (3.16),

$$S_1(x) = \frac{\pi F^2}{4L^2} \int_{-\infty}^{\infty} \frac{E_4(k) \sinh(k\lambda_2) [\sin k(x + L) - \sin k(x - L)]}{(\pi^2/L^2 - k^2) E_5(k)} dk \tag{3.18}$$

and

$$Q_1(x) = \frac{\pi \gamma_2^2 F^4}{4L^2} \int_{-\infty}^{\infty} \frac{k \sinh(k\lambda_1) \sinh(k\lambda_2) [\sin k(x + L) - \sin k(x - L)]}{(\pi^2/L^2 - k^2) E_5(k)} dk. \tag{3.19}$$

Note that

$$E_5(k) = 0 \tag{3.20}$$

represents the *dispersion relation* for this linearized problem. The present study determines the nature of the roots of this dispersion relation with the help of Rouché’s theorem. The detailed derivation, which was not reported in earlier studies [6], is given in the **Appendix**. The dispersion relation (3.20) for the case of three-layer fluid has two positive real roots, say k_0 and k_1 . It is to be noted that $-k_0$ and $-k_1$ are also roots of the relation (3.20).

The integrals in (3.18) and (3.19) are singular with poles on the real axis at $k = \pm k_0, \pm k_1$. Henceforth, these integrals have to be understood as Cauchy principal values, with an indentation below the singularities at $k = \pm k_0, \pm k_1$. Hence,

$$S_1(x) = \begin{cases} \frac{-\pi^2 F^2}{L^2} \sum_{j=0}^1 \frac{E_4(k_j) \sinh(k_j \lambda_2)}{(\pi^2/L^2 - k_j^2) E_5'(k_j)} \sin k_j x \sin k_j L & \text{for } x > L, \\ 0 & \text{for } x < -L \end{cases} \tag{3.21}$$

and

$$Q_1(x) = \begin{cases} \frac{-\pi^2 F^4 \gamma_2^2}{L^2} \sum_{j=0}^1 \frac{k_j \sinh(k_j \lambda_1) \sinh(k_j \lambda_2)}{(\pi^2/L^2 - k_j^2) E_5'(k_j)} \sin k_j x \sin k_j L & \text{for } x > L, \\ 0 & \text{for } x < -L. \end{cases} \tag{3.22}$$

From (3.21) and (3.22), we have observed that $S_1(x)$ and $Q_1(x)$ are oscillatory in nature, representing waves of two different wave numbers. The existence of two different wave numbers is mainly due to two positive real roots of the dispersion relation (3.20). In addition, we have found that these waves are propagating downstream and there is no wave upstream. The most important observation here is that the amplitudes of the waves having distinct wave numbers are varying. Further, several interesting features due to the varying amplitude may occur, which are illustrated later in Section 5. For example:

- (a) for certain speed ratios the wavy solutions may cancel out, and these might be close to wave-free solutions. This happens if the change in amplitude is not too large (refer to Figures 4(a) and 6(b), described in Section 5);
- (b) also, we have found a beating-like behaviour giving rise to a third wave whose amplitude is larger than the two waves observed (refer to Figure 6, described in Section 5);
- (c) there can be a downstream resonance for certain values of the parameters involved in the study.

Here it may be noted that in the case of a two-layer fluid where the upper fluid layer is bounded by a rigid lid [6], there exists a propagating wave of constant amplitude and of one wave number. Hence, the features described in the present case are not reported in that article [6], because these are not possible in the case of two-layer fluid with the uppermost layer being bounded by a rigid lid.

EXAMPLE 3.2 (Convex bottom profile). In order to illustrate the behaviour of interface profiles due to the influence of a convex bottom profile, we further consider a smooth convex bottom profile given by

$$f(x) = \begin{cases} (x^2 - L^2) & \text{when } |x| \leq L, \\ 0 & \text{when } |x| > L. \end{cases} \tag{3.23}$$

In this context,

$$a(k) = \frac{8F^2[kL \cos(kL) - \sin(kL)]E_4(k) \sinh(k\lambda_2)}{\pi k^2 E_5(k)},$$

$$b(k) = \frac{8F^4 \gamma_2^2 [kL \cos(kL) - \sin(kL)] \sinh(k\lambda_1) \sinh(k\lambda_2)}{\pi k E_5(k)}.$$

Hence, from (3.16),

$$S_1(x) = \frac{2F^2 L}{\pi} \int_{-\infty}^{\infty} \frac{E_4(k) \sinh(k\lambda_2) [\cos k(x + L) + \cos k(x - L)]}{k E_5(k)} dk$$

$$- \frac{2F^2}{\pi} \int_{-\infty}^{\infty} \frac{E_4(k) \sinh(k\lambda_2) [\sin k(x + L) + \sin k(x - L)]}{k^2 E_5(k)} dk \tag{3.24}$$

and

$$Q_1(x) = \frac{2F^4 \gamma_2^2 L}{\pi} \int_{-\infty}^{\infty} \frac{\sinh(k\lambda_1) \sinh(k\lambda_2) [\cos k(x + L) + \cos k(x - L)]}{E_5(k)} dk$$

$$- \frac{2F^4 \gamma_2^2}{\pi} \int_{-\infty}^{\infty} \frac{\sinh(k\lambda_1) \sinh(k\lambda_2) [\sin k(x + L) + \sin k(x - L)]}{k E_5(k)} dk. \tag{3.25}$$

After using the residue theorem [4] in (3.24) and (3.25),

$$S_1(x) = \begin{cases} -8F^2L \sum_{j=0}^1 \frac{E_4(k_j) \sinh(k_j\lambda_2)}{k_j E'_5(k_j)} \sin k_j x \cos k_j L \\ \quad + 8F^2 \sum_{j=0}^1 \frac{E_4(k_j) \sinh(k_j\lambda_2)}{k_j^2 E'_5(k_j)} \cos k_j x \cos k_j L & \text{for } x > L, \\ 0 & \text{for } x < -L, \end{cases} \tag{3.26}$$

$$Q_1(x) = \begin{cases} -8F^4\gamma_2^2L \sum_{j=0}^1 \frac{\sinh(k_j\lambda_1) \sinh(k_j\lambda_2)}{E'_5(k_j)} \sin k_j x \cos k_j L \\ \quad + 8F^4\gamma_2^2 \sum_{j=0}^1 \frac{\sinh(k_j\lambda_1) \sinh(k_j\lambda_2)}{k_j E'_5(k_j)} \cos k_j x \cos k_j L & \text{for } x > L, \\ 0 & \text{for } x < -L. \end{cases} \tag{3.27}$$

Note that in the case of a convex profile, similar observations are noticed concerning waves of variable amplitudes propagating downstream with no wave upstream.

3.4. Validation of the present results To validate this model, the present results are compared with the existing results available in the literature. To the authors' knowledge, only the theoretical results of the problem involving fluid flow over undulating bottom topography in a two-layer fluid are available in the literature. Therefore, the study is carried out by validating the results of the two-layer fluid flow over an undulating bottom only.

Observe that the three-layer fluid flow problem becomes a two-layer fluid flow problem in the absence of an uppermost layer, that is, when $\rho_3 = 0, H_3 = 0$ and $c_3 = 0$. To validate the present model, we derived the results by taking $\rho_3 = 0, H_3 = 0$ and $c_3 = 0$. We found that $\phi_{31}(x, y)$ and $Q_1(x)$ disappeared since $\gamma_1 = 0$, and the other results were

$$\phi_{21}(x, y) = \int_0^\infty \frac{\gamma_2 a(k)}{\sinh(k\lambda_2)} \cosh k(y - 1 - \lambda_2) \sin(kx) dk,$$

$$\phi_{11}(x, y) = \int_0^\infty \left[\frac{M(k) - a(k) \cosh k}{\sinh k} \cosh k(y - 1) - a(k) \sinh k(y - 1) \right] \sin(kx) dk$$

and

$$S_1(x) = \frac{\pi F^2}{4L^2} \int_{-\infty}^\infty \frac{\sinh(k\lambda_2) [\sin k(x + L) - \sin k(x - L)]}{(\pi^2/L^2 - k^2)E(k)} dk,$$

where

$$E(k) = F^2 k D_2 \gamma_2^2 \sinh k \cosh(k\lambda_2) + [F^2 k \cosh k - (1 - D_2) \sinh k] \sinh(k\lambda_2),$$

which exactly matched the results for the problem involving two-layer fluid flow over a concave bottom with the uppermost layer being bounded by a rigid lid, as considered by Belward and Forbes [2] and Chakrabarti and Martha [6].

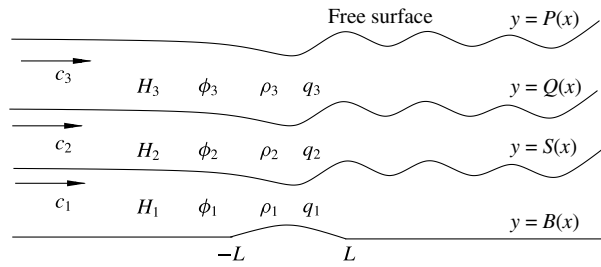


FIGURE 2. Definition sketch of wave propagation where the uppermost layer is free to the atmosphere.

4. Three-layer flow when the uppermost layer is free to the atmosphere

In this section, the same problem described in Section 3 is considered with the uppermost fluid layer free to the atmosphere instead of the rigid-lid approximation. The fluid system is shown schematically in Figure 2.

4.1. Mathematical formulation The following BVPs need to be solved for obtaining the velocity potentials and profiles of the interface and free surface. The velocity potentials ϕ_j ($j = 1, 2, 3$) satisfy Laplace’s equation:

$$\nabla^2 \phi_j = 0 \quad \text{for } j = 1, 2, 3.$$

At the free surface, Bernoulli’s condition is

$$\frac{1}{2} F^2 (q_3^2 - \gamma_1^2) + P(x) = 1 + \lambda_1 + \lambda_2 \quad \text{on } y = P(x).$$

By assuming no flow across the free surface, we obtain the condition

$$\phi_{3,n} = 0 \quad \text{on } y = P(x).$$

The conditions on the interfaces and at the bottom are the same as the conditions (3.3)–(3.7). The conditions far upstream (when $x \rightarrow -\infty$) are

$$\begin{aligned} \vec{q}_3 &\rightarrow \gamma_1 \vec{i}, & \vec{q}_2 &\rightarrow \gamma_2 \vec{i}, & \vec{q}_1 &\rightarrow \vec{i}, & S(x) &\rightarrow 1, & Q(x) &\rightarrow 1 + \lambda_2, \\ & & & & & & P(x) &\rightarrow 1 + \lambda_2 + \lambda_1. \end{aligned}$$

We solve these BVPs in the next subsection.

4.2. Method of solution and results The method of solution and results for the problem involving three-layer flow with a free surface are based on the analysis given earlier in Subsection 3.2. We assume the similar bottom profile as mentioned earlier in Section 3. Next, we express the velocity potentials and the interface profiles in terms of the perturbation parameter ϵ as given by the relations (3.9)–(3.13). In addition to the earlier expressions (3.9)–(3.13), the profile of the free surface is expressed as

$$P(x) = 1 + \lambda_2 + \lambda_1 + \epsilon P_1(x) + O(\epsilon^2).$$

Employing similar analysis as described in Subsection 3.2, we obtain the first-order potentials

$$\begin{aligned} \phi_{31}(x, y) &= \int_0^\infty \left[\frac{\gamma_1 [b(k) - c(k) \cosh k\lambda_1]}{\sinh k\lambda_1} \cosh k(y - 1 - \lambda_1 - \lambda_2) \right. \\ &\quad \left. - \gamma_1 c(k) \sinh k(y - 1 - \lambda_1 - \lambda_2) \right] \sin(kx) dk, \\ \phi_{21}(x, y) &= \int_0^\infty \left[\frac{\gamma_2 [a(k) - b(k) \cosh(k\lambda_2)]}{\sinh(k\lambda_2)} \cosh k(y - 1 - \lambda_2) \right. \\ &\quad \left. - \gamma_2 b(k) \sinh k(y - 1 - \lambda_2) \right] \sin(kx) dk, \\ \phi_{11}(x, y) &= \int_0^\infty \left[\frac{M(k) - a(k) \cosh k}{\sinh k} \cosh k(y - 1) - a(k) \sinh k(y - 1) \right] \sin(kx) dk, \end{aligned}$$

where

$$\begin{aligned} a(k) &= \frac{F^2 k M(k) E_7(k) \sinh(k\lambda_2)}{E_8(k)}, \\ b(k) &= \frac{F^2 \gamma_2^2 a(k) k E_6(k) \sinh(k\lambda_1)}{E_7(k)}, \\ c(k) &= \frac{F^2 \gamma_1^2 b(k)}{E_6(k)}, \end{aligned} \tag{4.1}$$

with

$$\begin{aligned} E_6(k) &= \frac{1}{k} [F^2 \gamma_1^2 k \cosh(k\lambda_1) - \sinh(k\lambda_1)], \\ E_7(k) &= [\gamma_2^2 F^2 k \cosh(k\lambda_2) \sinh(k\lambda_1) + \gamma_1^2 F^2 k D_1 \cosh(k\lambda_1) \sinh(k\lambda_2) \\ &\quad - (1 - D_1) \sinh(k\lambda_1) \sinh(k\lambda_2)] E_6(k) - F^4 \gamma_1^4 D_1 k \sinh(k\lambda_2), \\ E_8(k) &= E_7(k) \{ F^2 k \cosh k \sinh(k\lambda_2) + [\gamma_2^2 F^2 k D_2 \cosh(k\lambda_2) \\ &\quad - (1 - D_2) \sinh(k\lambda_2)] \sinh k \} - \gamma_2^4 F^4 k^2 E_6(k) D_2 \sinh k \sinh(k\lambda_1). \end{aligned}$$

4.3. Special forms of the bottom profiles This section is devoted to evaluating the profiles of the interfaces and free surface due to both kinds of bottom profiles, such as concave and convex.

EXAMPLE 4.1 (Concave bottom profile). We adopt a smooth concave bottom profile similar to the one considered in Section 3.3. The expressions for $a(k)$, $b(k)$ and $c(k)$ are obtained from (4.1) and, hence, are

$$S_1(x) = \frac{\pi F^2}{4L^2} \int_{-\infty}^\infty \frac{E_7(k) \sinh(k\lambda_2) [\sin k(x + L) - \sin k(x - L)]}{(\pi^2/L^2 - k^2) E_8(k)} dk, \tag{4.2}$$

$$Q_1(x) = \frac{\pi F^4 \gamma_2^2}{4L^2} \int_{-\infty}^\infty \frac{E_6(k) k \sinh(k\lambda_1) \sinh(k\lambda_2) [\sin k(x + L) - \sin k(x - L)]}{(\pi^2/L^2 - k^2) E_8(k)} dk \tag{4.3}$$

and

$$P_1(x) = \frac{\pi F^6 \gamma_1^2 \gamma_2^2}{4L^2} \int_{-\infty}^\infty \frac{\sinh(k\lambda_2) [\sin k(x + L) - \sin k(x - L)]}{(\pi^2/L^2 - k^2) E_8(k)} dk. \tag{4.4}$$

The dispersion relation of the above linearized problem is

$$E_8(k) = 0. \tag{4.5}$$

Applying similar analysis as in the case of the dispersion relation (3.20), we found that the dispersion relation (4.5) has three positive real roots, k_0, k_1 and k_2 (say). Using the residue theorem in relations (4.2)–(4.4) with an indented contour below the poles at $k = \pm k_0, \pm k_1, \pm k_2$,

$$S_1(x) = \begin{cases} \frac{-\pi^2 F^2}{L^2} \sum_{j=0}^2 \frac{E_7(k_j) \sinh(k_j \lambda_2)}{(\pi^2/L^2 - k_j^2) E_8'(k_j)} \sin k_j x \sin k_j L & \text{for } x > L, \\ 0 & \text{for } x < -L, \end{cases} \tag{4.6}$$

$$Q_1(x) = \begin{cases} \frac{-\pi^2 F^4 \gamma_2^2}{L^2} \sum_{j=0}^2 \frac{E_6(k_j) k_j \sinh(k_j \lambda_1) \sinh(k_j \lambda_2)}{(\pi^2/L^2 - k_j^2) E_8'(k_j)} \sin k_j x \sin k_j L & \text{for } x > L, \\ 0 & \text{for } x < -L \end{cases} \tag{4.7}$$

and

$$P_1(x) = \begin{cases} \frac{-\pi^2 F^6 \gamma_1^2 \gamma_2^2}{L^2} \sum_{j=0}^2 \frac{\sinh(k_j \lambda_2)}{(\pi^2/L^2 - k_j^2) E_8'(k_j)} \sin k_j x \sin k_j L & \text{for } x > L, \\ 0 & \text{for } x < -L. \end{cases} \tag{4.8}$$

EXAMPLE 4.2 (Convex bottom profile). An approach similar to the one in Section 3.3 is followed to evaluate the influence of the convex bottom profile on the profiles of the interfaces and free surface. The same convex bottom profile as given in (3.23) is considered. Next, using similar analysis to that discussed earlier, we have obtained the first-order profiles

$$S_1(x) = \begin{cases} -8F^2 L \sum_{j=0}^2 \frac{E_7(k_j) \sinh(k_j \lambda_2)}{k_j E_8'(k_j)} \sin k_j x \cos k_j L \\ + 8F^2 \sum_{j=0}^2 \frac{E_7(k_j) \sinh(k_j \lambda_2)}{k_j^2 E_8'(k_j)} \cos k_j x \cos k_j L & \text{for } x > L, \\ 0 & \text{for } x < -L, \end{cases} \tag{4.9}$$

$$Q_1(x) = \begin{cases} -8F^4 \gamma_2^2 L \sum_{j=0}^2 \frac{E_6(k_j) \sinh(k_j \lambda_1) \sinh(k_j \lambda_2)}{E_8'(k_j)} \sin k_j x \cos k_j L \\ + 8F^4 \gamma_2^2 \sum_{j=0}^2 \frac{E_6(k_j) \sinh(k_j \lambda_1) \sinh(k_j \lambda_2)}{k_j E_8'(k_j)} \cos k_j x \cos k_j L & \text{for } x > L, \\ 0 & \text{for } x < -L \end{cases} \tag{4.10}$$

and

$$P_1(x) = \begin{cases} -8F^6\gamma_1^2\gamma_2^2L \sum_{j=0}^2 \frac{\sinh(k_j\lambda_2)}{k_jE'_8(k_j)} \sin k_jx \cos k_jL \\ \quad + 8F^6\gamma_1^2\gamma_2^2 \sum_{j=0}^2 \frac{\sinh(k_j\lambda_2)}{k_j^2E'_8(k_j)} \cos k_jx \cos k_jL & \text{for } x > L, \\ 0 & \text{for } x < -L. \end{cases} \tag{4.11}$$

From the expressions (4.6)–(4.11), we observe that the interfaces $S_1(x)$, $Q_1(x)$ and the free surface $P_1(x)$ are oscillatory in nature. In addition, each of the two interfaces and the free surface possesses a wave train, which comprises three waves having different wave numbers downstream of the obstacle. However, the upstream region of the obstacle is a wave-free zone. Different wave numbers are due to the existence of three real positive roots of the dispersion relation (4.5). Similar observations as discussed in Section 3.3 are noticed in the present case regarding the amplitude and other interesting features of the resulting waves occurring due to the superposition of three waves with different wave numbers. The interesting features for the present case are discussed in Section 5.

4.4. Validation of the present results In a similar way as discussed in Section 3.4, the present results are validated with the results for fluid flow over an undulating bottom in a two-layer system as available in the literature. Therefore, a comparison is established with the theoretical results of Chakrabarti and Martha [6] and the current work. In the absence of the uppermost layer, $\phi_{31}(x, y)$ and $P_1(x)$ disappear, and

$$\begin{aligned} \phi_{21}(x, y) &= \int_0^\infty \left[\frac{\gamma_2 a(k) - b(k) \cosh k\lambda_2}{\sinh(k\lambda_2)} \cosh k(y - 1 - \lambda_2) \right. \\ &\quad \left. - \gamma_2 b(k) \sinh k(y - 1 - \lambda_2) \right] \sin(kx) dk, \\ \phi_{11}(x, y) &= \int_0^\infty \left[\frac{M(k) - a(k) \cosh k}{\sinh k} \cosh k(y - 1) - a(k) \sinh k(y - 1) \right] \sin(kx) dk, \\ S_1(x) &= \frac{\pi F^2}{4L^2} \int_{-\infty}^\infty \frac{E_1(k) \sinh(k\lambda_2) [\sin k(x + L) - \sin k(x - L)]}{(\pi^2/L^2 - k^2)E_2(k)} dk, \\ Q_1(x) &= \frac{\pi F^4 \gamma_2^2}{4L^2} \int_{-\infty}^\infty \frac{\sinh(k\lambda_2) [\sin k(x + L) - \sin k(x - L)]}{(\pi^2/L^2 - k^2)E_2(k)} dk, \end{aligned}$$

where

$$\begin{aligned} E_2(k) &= E_1(k) [F^2 k \cosh k \sinh(k\lambda_2) + \{F^2 D_2 \gamma_2^2 k \cosh(k\lambda_2) \\ &\quad - (1 - D_2) \sinh(k\lambda_2)\} \sinh k] - F^4 D_2 \gamma_2^4 k \sinh k, \end{aligned}$$

with $E_1(k) = [F^2 \gamma_2^2 k \cosh(k\lambda_2) - \sinh(k\lambda_2)]/k$.

It is clear that when there is no uppermost fluid layer, the results are in agreement with the results of Chakrabarti and Martha [6].

TABLE 1. Wave numbers k for a fluid flow when the uppermost layer is bounded by a rigid lid.

Values of the parameters	Wave number: three-layer	Wave number: two-layer [2]
$F = 0.2, \lambda_1 = 1, \lambda_2 = 1$	4.355 12 4.461 24	4.410 46
$F = 0.3, \lambda_1 = 1, \lambda_2 = 1$	1.409 93 2.145 86	1.869 75
$F = 0.2, \lambda_1 = 2, \lambda_2 = 1$	4.355 59 4.461 53	4.410 46
$F = 0.3, \lambda_1 = 1, \lambda_2 = 2$	1.861 42 1.951 30	1.909 62
$F = 0.3, \lambda_1 = 2, \lambda_2 = 2$	1.883 03 1.98024	1.909 62

5. Results and discussion

This section comprises a discussion about the roots (wave numbers, k) of the dispersion relation and the behaviour of interface profiles for both flow problems. In addition, it also contains the effect of different system parameters like obstacle height, obstacle length, density ratios and so on on the quantities of interest, namely the profiles of interfaces. Several computations are performed and, in particular, some special results are tabulated and presented in graphical form. In the present study, the Froude number $F = 0.3$, ratios of fluid depth $\lambda_1 = 1, \lambda_2 = 1$, ratios of density $D_1 = 0.7, D_2 = 0.7$, ratios of upstream speed $\gamma_1 = 1, \gamma_2 = 1$, length of obstacle $L = 0.5$ and height of obstacle $\varepsilon = 0.6$, which are kept fixed for computation unless otherwise mentioned in the text.

5.1. Wave numbers with effect of different dimensionless parameters The numerical values of the roots (that is, wave numbers) of the two dispersion relations (3.20) and (4.5) are shown in Tables 1 and 2, respectively, for different combinations of Froude number, F , and fluid depth ratios, λ_1 and λ_2 . These roots are obtained by using Newton's method, keeping other parameters constant.

From Table 1, it is clear that the dispersion relation (3.20) has two nonzero real positive roots as verified in Section 3.3. Note that when $\gamma_1 = 0, \lambda_1 = 0$ and $D_1 = 0$, the dispersion relation (3.20) reduces to the same one for two-layer flow, when the uppermost layer is bounded by a rigid lid [2]. We have calculated the roots of the relation (3.20) by taking $\gamma_1 = 0, \lambda_1 = 0$ and $D_1 = 0$ and they are shown in Table 1 (refer to the last column). In this particular case, we have successfully obtained one wave number, which is similar to a previous study [2]. Further, from the present work, we have also noticed that the wave number decreases as the value of the Froude number, F , increases. From Table 1, observe that there is an insignificant increment in both wave

TABLE 2. Wave numbers k for a fluid flow when the uppermost layer is free to the atmosphere.

Values of the parameters	Wave number: three-layer	Wave number: two-layer [6]
$F = 0.2, \lambda_1 = 1, \lambda_2 = 1$	4.355 15	4.410 23
	4.461 19	24.40 86
	25.00 00	
$F = 0.3, \lambda_1 = 1, \lambda_2 = 1$	1.409 91	1.851 19
	2.145 82	11.10 12
	11.11 10	
$F = 0.2, \lambda_1 = 2, \lambda_2 = 1$	4.355 59	4.410 25
	4.461 52	24.41 24
	25.00 14	
$F = 0.3, \lambda_1 = 2, \lambda_2 = 2$	1.883 04	1.909 28
	1.980 23	11.11 32
	11.11 11	

numbers due to the upstream depth ratio λ_1 . However, there is a significant increase in the lower wave number and a significant decrease in the higher wave number due to the upstream depth ratio λ_2 . Our study reveals that the wave numbers are somewhat insensitive to the depth λ_1 of the upper layer fluid, but sensitive to the depth λ_2 of the middle layer fluid. In addition, the difference between two wave numbers decreases as the fluid depth ratio, λ_2 , increases. This phenomenon indicates that as the depth ratio increases, the downstream waves having variable amplitude may become waves with constant amplitude. In the case of three-layer fluid flow having a free surface, the roots of the dispersion relation (4.5) are shown in Table 2. It is clear from Table 2 that the dispersion relation (4.5) has three nonzero positive real roots, which confirms the theoretical investigation analysed in Section 4.3. A similar phenomenon concerning the effect of the Froude number is also observed in the case of three-layer flow having a free surface.

5.2. Effect of dimensionless parameters on the profiles for flow with rigid lid

In the case of three-layer fluid flow over a *concave* bottom with the uppermost layer having a rigid lid, the interface profiles $S(x)$ and $Q(x)$ are evaluated using the relations (3.12), (3.13), (3.21) and (3.22). However, in the case of a *convex* bottom, the interface profiles are evaluated using the relations (3.12), (3.13), (3.26) and (3.27). In Figure 3(a), the interface profile $S(x)$ due to a *concave* as well as a *convex* bottom is shown for different values of obstacle height ε , while Figure 3(b) depicts the interface profile $Q(x)$ due to both bottom profiles. In both figures, the interface profiles for a concave bottom are shown in black lines, whereas the profiles for a convex bottom are indicated by blue lines. The common feature observed in both Figure 3(a) and (b) is that the profiles are oscillatory in nature (representing waves). The oscillatory

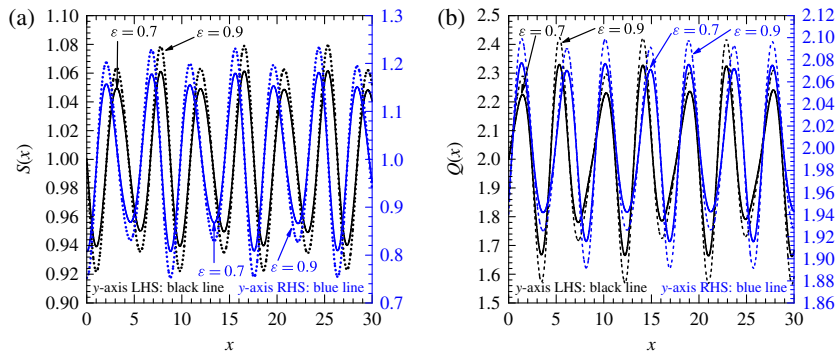


FIGURE 3. Variation of the profiles (flow when the uppermost layer is bounded by a rigid lid) due to *concave* and *convex* bottom for different obstacle heights in (a) $S(x)$ and (b) $Q(x)$ for $F = 0.3$, $\gamma_1 = 1$, $\gamma_2 = 1$, $\lambda_1 = 1$, $\lambda_2 = 1$, $D_1 = 0.7$, $D_2 = 0.7$ and $L = 1$. The profiles for a *concave* bottom are indicated by black lines with the scale shown in the left hand side axis and the same for a *convex* bottom are indicated by blue lines with scale shown in the right hand side axis. (Colour available online.)

nature may be attributed to multiple interactions of the fluid with the bottom and the interfaces. In addition, the amplitude of each profile increases with the height of the obstacle, as illustrated in Figure 3. This agrees with physical intuition, since a high obstacle will produce waves with higher amplitude. In comparison with earlier papers (see, for example, [6]), the present study reveals that the amplitude of each profile is varying. This varying nature is due to the fact that more waves of different wave numbers propagate with the same speed. Further, in Figure 3, we have also observed that for the particular parameter values, the downstream wave has a beating-like behaviour. As a result, every third wave has an amplitude larger than the two previous waves. This is completely consistent with our theoretical observation as described in Section 3. The occurrence of beating-like behaviour is mainly due to the existence of two different frequencies in the downstream waves.

The outcome of the effect of density ratios on the interface profiles is shown in Figure 4(a) and (b). Figure 4(a) demonstrates the profile $S(x)$ and Figure 4(b) demonstrates the profile $Q(x)$. From Figure 4(a) and (b), observe that the amplitude of the downstream amplitude-modulated waves, $S(x)$ and $Q(x)$, gradually reduces as the density ratio reduces. This may be attributed to the fact that the densities of the two layers across the profiles differ. Since the amplitude of the downstream waves decreases, it may happen that a closely wave-free solution (refer to Figure 4(a)) exists for particular values of the parameters involved in the study. Further, one can also visualize from Figure 4(a) and (b) that the wavelength of the profiles reduces (that is, wave number increases) as the density ratio reduces. For illustration purposes, the results are presented for a concave bottom only. A similar phenomenon is also observed in the case of a convex bottom, which can be determined in a similar fashion.

We have also investigated the effect of the obstacle length on the interface profiles $S(x)$ and $Q(x)$, and this is shown in Figure 5(a)–(d) for various values of the length

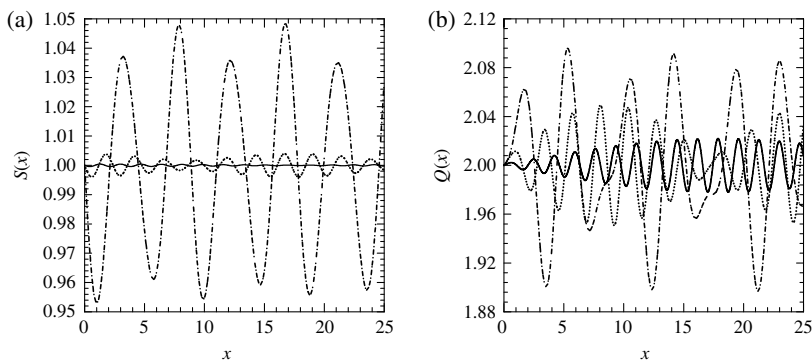


FIGURE 4. Variation of the profiles (flow when the uppermost layer is bounded by a rigid lid) in (a) $S(x)$ and (b) $Q(x)$ due to a *concave* bottom for $F = 0.3$, $\gamma_1 = 1$, $\gamma_2 = 1$, $\lambda_1 = 1$, $\lambda_2 = 1$, $L = 0.5$ and $\varepsilon = 0.9$. The profiles are for $D_1 = 0.7 = D_2$ (chain line), $D_1 = 0.6 = D_2$ (dashed line) and $D_1 = 0.4 = D_2$ (solid line).

of the obstacle situated at the bottom. Figure 5(a) and (b) correspond to the interface profiles due to a *concave* bottom, whereas the profiles due to a *convex* bottom are shown in Figure 5(c) and (d). It can be observed from Figure 5(a) and (b) that the amplitude of the downstream waves increases up to a certain length L of the obstacle, but after that the amplitude of the waves decreases when the length increases. As a result, the wavy nature of the profiles diminishes with a certain length. In the present study, we have observed that the amplitude increases up to $L = 1.7$, the amplitude is nearly the same in the range $L = 1.8$ to $L = 2.1$ and the amplitude decreases for $L > 2.1$. In the case of a *convex* bottom, as expected, the amplitude of the downstream waves decreases up to a certain length L of the obstacle and, then, the amplitude increases with obstacle length as shown in Figure 5(c) and (d).

To illustrate the effect of varying upstream speed ratios, the interface profiles $S(x)$ and $Q(x)$ for a *concave* as well as a *convex* bottom are plotted in Figure 6 for two different sets of upstream speed ratios: $\gamma_1 = 0.75$, $\gamma_2 = 0.75$ and $\gamma_1 = 1$, $\gamma_2 = 1$. We have observed, in both Figure 6(a) and (b), the beating-like behaviour for the particular values of the various parameters. In addition, we have also found (refer to Figure 6(a)) the existence of a closely wave-free solution for particular values of the parameters involved in the study. Further, we have also observed that both the amplitude and wavelength of the downstream waves increase as the ratio of upstream fluid speed increases. This phenomenon can be realized from the dispersion relation (3.20), by increasing the values of the upstream speed ratio and noticing the corresponding decrease in the values of wave number (that is, an increase of wavelength). This observation is completely consistent with the results presented by Belward and Forbes [2].

5.3. Effect of dimensionless parameters on the profiles for flow with free surface

The effect of different dimensionless parameters on the interface profiles $S(x)$ and $Q(x)$ and free-surface profile, $P(x)$, is illustrated in Figures 7–9. Figure 7(a)–(c) depict these

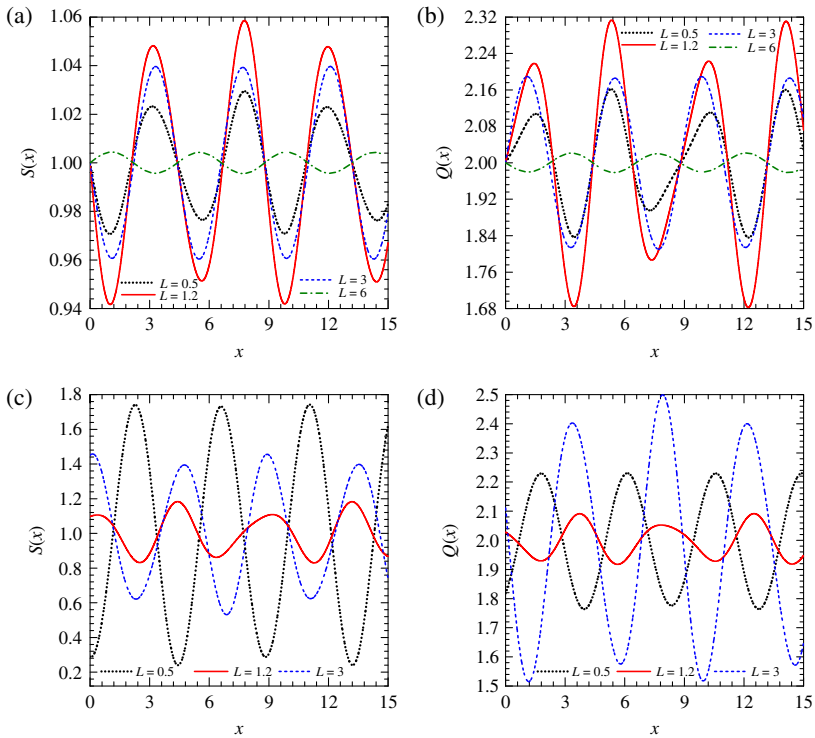


FIGURE 5. Variation of the profiles (flow when the uppermost layer is bounded by a rigid lid) in (a) $S(x)$ and (b) $Q(x)$ due to a *concave* bottom and in (c) $S(x)$ and (d) $Q(x)$ due to a *convex* bottom for various lengths of the obstacle with $F = 0.3$, $\gamma_1 = 1$, $\gamma_2 = 1$, $\lambda_1 = 1$, $\lambda_2 = 1$, $D_1 = 0.7$, $D_2 = 0.7$ and $\varepsilon = 0.6$. The profiles are for $L = 0.5$ (dotted black line), $L = 1.2$ (red solid line), $L = 3$ (blue dashed line) and $L = 6$ (green chain line). (Colour available online.)

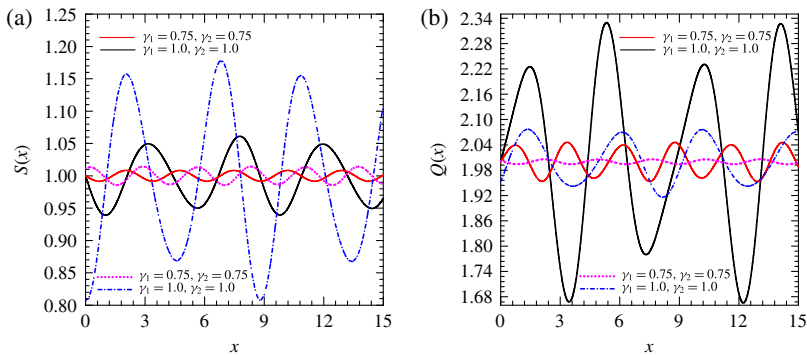


FIGURE 6. Variation of the profiles (flow when the uppermost layer is bounded by a rigid lid) in (a) $S(x)$ and (b) $Q(x)$ for different ratios of upstream fluid speed with $F = 0.3$, $\lambda_1 = 1$, $\lambda_2 = 1$, $D_1 = 0.7$, $D_2 = 0.7$, $L = 1$ and $\varepsilon = 0.7$. The profiles due to a *concave* bottom are indicated by a black solid line ($\gamma_1 = 1$, $\gamma_2 = 1$) and a red solid line ($\gamma_1 = 0.75$, $\gamma_2 = 0.75$). The profiles due to a *convex* bottom are indicated by a blue dotted line ($\gamma_1 = 1$, $\gamma_2 = 1$) and a magenta dotted line ($\gamma_1 = 0.75$, $\gamma_2 = 0.75$). (Colour available online.)

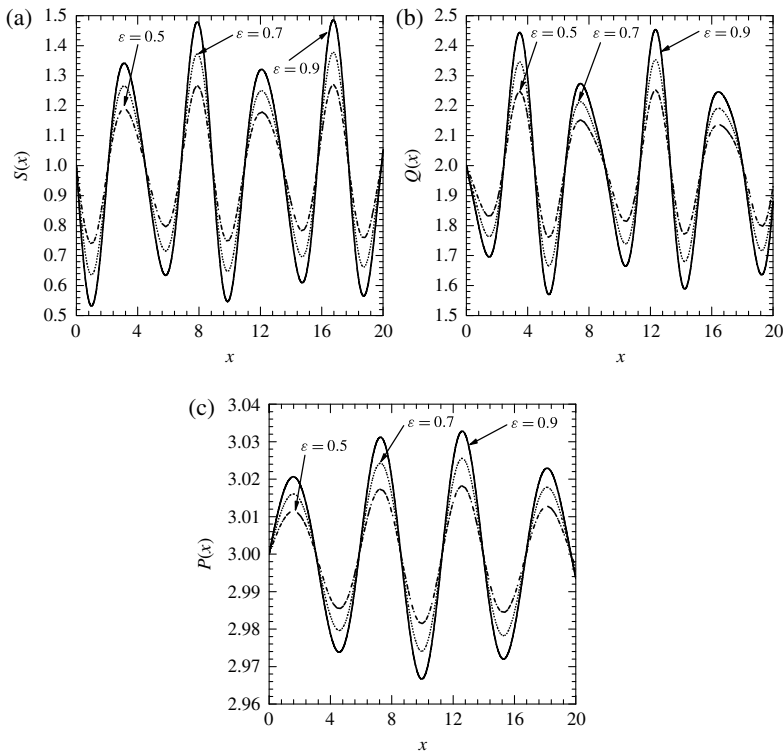


FIGURE 7. Variation of the profiles (flow when the uppermost layer is free to the atmosphere) in (a) $S(x)$, (b) $Q(x)$ and (c) $P(x)$ due to a *concave* bottom for different obstacle heights with $F = 0.3$, $\gamma_1 = 1$, $\gamma_2 = 1$, $\lambda_1 = 1$, $\lambda_2 = 1$, $D_1 = 0.7$, $D_2 = 0.7$ and $L = 0.5$.

profiles due to three-layer fluid flow over a *concave* bottom for three different values of the obstacle height, $\varepsilon = 0.5, 0.7$ and 0.9 . In accordance with the earlier observations in Figure 3, the present profiles $S(x)$, $Q(x)$ and $P(x)$ exhibit a similar oscillatory nature, and the amplitudes are found to be varying (refer to Figures 7 and 9). It can be seen from Figure 7(a)–(c) that the amplitudes of the amplitude-modulated waves $S(x)$, $Q(x)$ and $P(x)$ increase as the height of the obstacle situated at the undulating bottom increases. The reason for this phenomenon is the same as given earlier in Figure 3. In a similar way, analysis shows that these profiles due to a *convex* bottom are oscillatory in nature having variable amplitudes. In this case, it is also noticed that the amplitudes of the profiles increase with the height of the obstacle.

Figure 8 depicts the influence of the obstacle length on the interface profiles of three-layer fluid flow over a *concave* bottom when the uppermost layer is free to the atmosphere. In this figure, the variation of the downstream waves $S(x)$, $Q(x)$ and $P(x)$ is presented for a similar set of parameters as that of the fluid flow when the uppermost layer is bounded by a rigid lid (Figure 5). The study reveals a similar observation as that of the previous study of three-layer fluid flow with a rigid lid (refer to Figure 5(a))

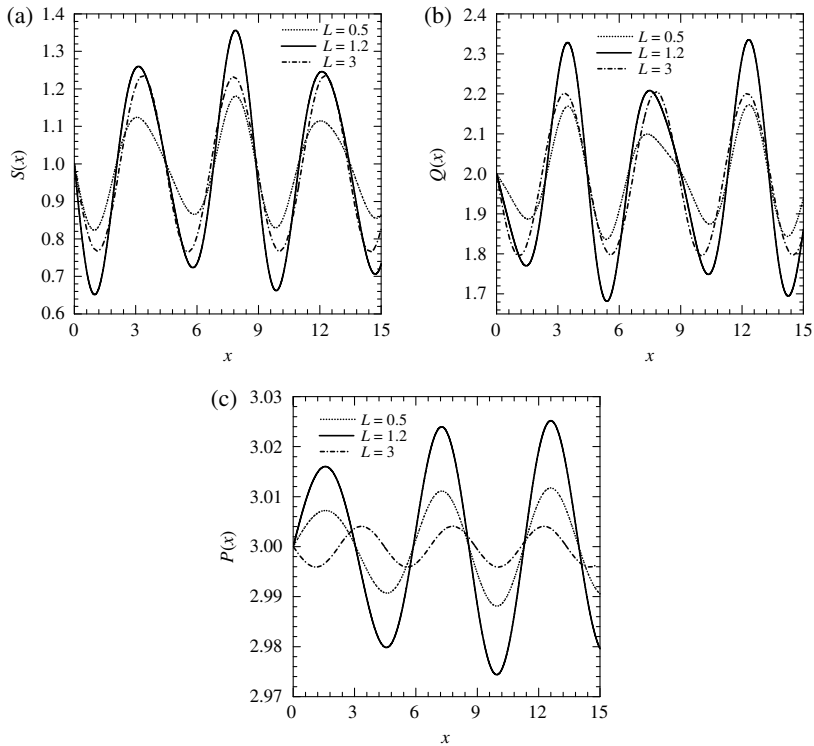


FIGURE 8. Variation of the profiles (flow when the uppermost layer is free to the atmosphere) in (a) $S(x)$, (b) $Q(x)$ and (c) $P(x)$ due to a *concave* bottom for various lengths of the obstacle with $F = 0.3$, $\gamma_1 = 1$, $\gamma_2 = 1$, $\lambda_1 = 1$, $\lambda_2 = 1$, $D_1 = 0.7$, $D_2 = 0.7$ and $\varepsilon = 0.6$.

and (b)). In a similar way as in Figure 8, the effect of the obstacle length on the amplitude of the downstream waves due to a *convex* bottom can also be studied.

The effect of two different sets of upstream speed ratios, that is, $\gamma_1 = 0.75$, $\gamma_2 = 0.75$ and $\gamma_1 = 1$, $\gamma_2 = 1$, on the free surface as well as interface profiles for both kinds of bottom profiles are illustrated in Figure 9. In Figure 9, the red solid line is chosen for the graphical representation of the profiles due to a *concave* bottom for $\gamma_1 = 1$, $\gamma_2 = 1$ and the black solid line is chosen for the graphical representation of the same for $\gamma_1 = 0.75$, $\gamma_2 = 0.75$. The magenta dotted line is chosen for the graphical representation of the profiles due to a *convex* bottom for $\gamma_1 = 1$, $\gamma_2 = 1$ and the blue dotted line is chosen for the graphical representation of the same for $\gamma_1 = 0.75$, $\gamma_2 = 0.75$. In Figure 9(a), we have noticed that, for certain values of the parameters, the wave solution leads to a nearly wave-free solution. This is consistent with the theoretical argument described earlier. Further, it is clear from Figure 9(a)–(c) that for both kinds of bottom profiles, the maximum amplitudes of the downstream waves $S(x)$, $Q(x)$ and $P(x)$ increase as the upstream speed ratio increases. Further, we also observe from Figure 9(a)–(c) that the wavelengths of the downstream waves $S(x)$, $Q(x)$ and

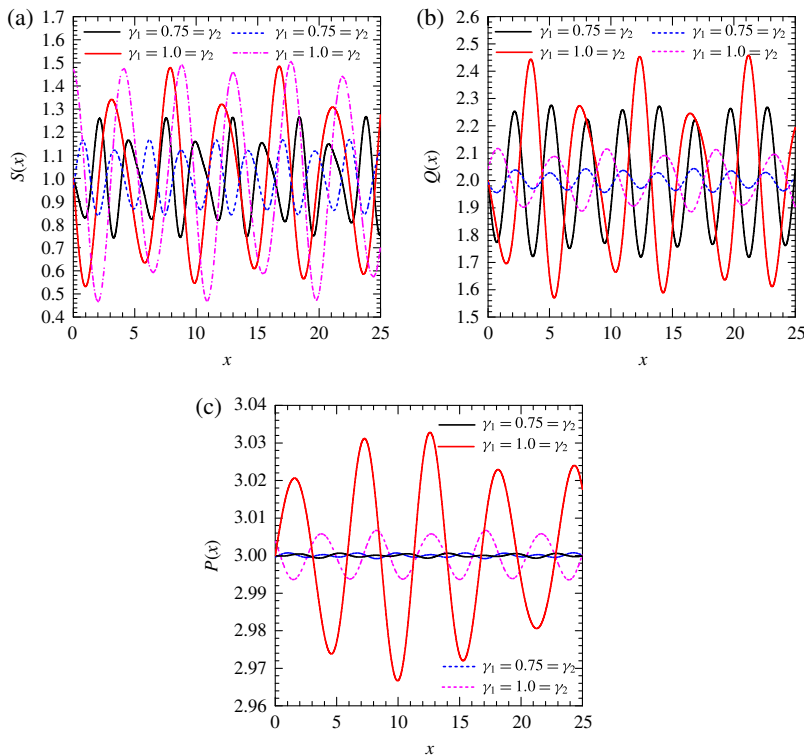


FIGURE 9. Profiles (flow when the uppermost layer is free to the atmosphere) in (a) $S(x)$, (b) $Q(x)$ and (c) $P(x)$ for different upstream speed ratios with $F = 0.3$, $\lambda_1 = 1$, $\lambda_2 = 1$, $D_1 = 0.7$, $D_2 = 0.7$, $L = 1$ and $\varepsilon = 0.5$. The profiles due to a *concave* bottom are indicated by a red solid line for $\gamma_1 = 1$, $\gamma_2 = 1$ and a black solid line for $\gamma_1 = 0.75$, $\gamma_2 = 0.75$. The profiles due to a *convex* bottom are indicated by a magenta dotted line for $\gamma_1 = 1$, $\gamma_2 = 1$ and a blue dotted line for $\gamma_1 = 0.75$, $\gamma_2 = 0.75$. (Colour available online.)

$P(x)$ due to both bottom profiles increase as the ratios of the upstream speed increase. Also, this fact can be visualized from the dispersion relation (4.5) for the reason that when the values of the ratio of upstream fluid speed decrease, the values of the wave number increase.

6. Conclusion

Flow problems involving three-layer fluid in an infinite channel over concave and convex bottom profiles were studied, where the uppermost fluid layer is either bounded by a rigid lid or free to the atmosphere. The interfaces which vary with x were considered as important practical parts of the formulation. The effect of surface tension was neglected. Perturbation analysis followed by the Fourier transform technique was employed to derive the first-order velocity potentials and profiles of the interfaces. The main advantage of this method is that we solved comparatively easier ordinary

differential equations. From the obtained results, it is clear that the profiles are oscillatory in nature, representing waves of variable amplitude with different wave numbers which lead to several interesting features, such as beating-like behaviour, a wave-free solution for certain values of the parameters and so on. In addition, the interfaces consist of a wave-free region upstream of the obstacle, followed by waves downstream. Further, the amplitudes of the profiles seem to be increasing with the height of the obstacle situated at the bottom. We also observed that the solution consists of several waves with variable amplitudes and of different wave numbers. This is in contrast with the situation which involves two-layer fluids, where the waves propagate downstream with one wave number and constant amplitude. We then predicted that in the case of multiple layers of fluids involving more than three layers, one should observe the existence of waves propagating downstream with variable amplitude and of many more distinct wave numbers, regardless of whether the bottom surface is concave or convex. Notice that although the flow in three layers of fluids is a natural extension of two layers of fluid, we have handled more complicated double-interface conditions occurring due to the presence of two interfaces. The present results may be helpful to analyse the mechanism of wave generation in a large class of multi-layered fluid flow problems over arbitrary bottom topography. As is well known, understanding channel flow problems considered in this paper is also useful in resolving various problems of atmospheric sciences [5, 20, 29, 30].

Acknowledgements

Srikumar Panda is grateful to the Council of Scientific and Industrial Research (CSIR), Government of India, for providing a Research Fellowship for pursuing a Ph.D. at the Indian Institute of Technology Ropar, India. S. C. Martha thanks I.I.T. Ropar for providing all the necessary facilities. Professor A. Chakrabarti thanks the National Academy of Sciences, India (NASI) for awarding him a Senior Scientists Platinum Jubilee Fellowship, which enabled him to pursue the present research. The authors express their deep sense of gratitude to the editor and the referees for their invaluable comments and suggestions which enabled them to carry out the desired revision of the manuscript.

Appendix

Assuming $\gamma_1 = \gamma_2 = 1$ and $D_1 = D_2 = D$ in the dispersion relation (3.20),

$$\begin{aligned} & [F^2 k \cosh(k\lambda_2) \sinh(k\lambda_1) + \{F^2 k D \cosh(k\lambda_1) - (1 - D) \sinh(k\lambda_1)\} \sinh(k\lambda_2)] \\ & \times [F^2 k \cosh k \sinh(k\lambda_2) + \{F^2 k D \cosh(k\lambda_2) - (1 - D) \sinh(k\lambda_2)\} \sinh k] \\ & - F^4 k^2 D \sinh k \sinh(k\lambda_1) = 0. \end{aligned} \quad (\text{A.1})$$

Now we will use Rouché's theorem to determine the nature of the roots of the relation (A.1).

Let us define

$$\begin{aligned}
 F(z) &= [F^2 z \cosh(z\lambda_2) \sinh(z\lambda_1) + \{F^2 z D \cosh(z\lambda_1) - (1 - D) \sinh(z\lambda_1)\} \sinh(z\lambda_2)] \\
 &\quad \times [F^2 z \cosh z \sinh(z\lambda_2) + \{F^2 z D \cosh(z\lambda_2) - (1 - D) \sinh(z\lambda_2)\} \sinh z] \\
 &= A(z) \times B(z) \text{ (say)}
 \end{aligned}$$

and

$$G(z) = -F^4 z^2 D \sinh(z) \sinh(z\lambda_1), \text{ where } z \text{ is complex.}$$

Let us consider the closed square contour C with vertices $((nb + \delta), (nb + \delta)), (-nb + \delta), (nb + \delta), (-nb + \delta), (-nb + \delta), (-nb + \delta), ((nb + \delta), -nb + \delta)$ in the complex z -plane, where n, b are integers and $\delta (> 0)$ is sufficiently small. The value of n is to be chosen in such a way that the contour C does not pass through any of the zeros of the function $F(z)$. The function $F(z)$ has four real roots (the analysis is given at the end of this section).

On the upper edge of the contour C , $z = x + i(nb + \delta)\pi$ and

$$\begin{aligned}
 \left| \frac{F(z)}{G(z)} \right| &= \left| \left[\frac{A(z)}{z} \times \frac{B(z)}{z} \right] \frac{G(z)}{z^2} \right| \\
 &= \left| \left[\left[F^2 \cosh \{ \lambda_2(x + i(nb + \delta)\pi) \} \sinh \{ \lambda_1(x + i(nb + \delta)\pi) \} \right. \right. \right. \\
 &\quad \left. \left. + \left\{ F^2 D \cosh \{ \lambda_1(x + i(nb + \delta)\pi) \} \right. \right. \right. \\
 &\quad \left. \left. - \frac{(1 - D) \sinh \{ \lambda_1(x + i(nb + \delta)\pi) \}}{\{x + i(nb + \delta)\pi\}} \right\} \sinh \{ \lambda_2(x + i(nb + \delta)\pi) \} \right] \\
 &\quad \times \left[F^2 \cosh \{x + i(nb + \delta)\pi\} \sinh \{ \lambda_2(x + i(nb + \delta)\pi) \} \right. \\
 &\quad \left. + \left\{ F^2 D \cosh \{ \lambda_2(x + i(nb + \delta)\pi) \} \right. \right. \\
 &\quad \left. \left. - \frac{(1 - D) \sinh \{ \lambda_2(x + i(nb + \delta)\pi) \}}{\{x + i(nb + \delta)\pi\}} \right\} \sinh \{x + i(nb + \delta)\pi\} \right] \Bigg| \\
 &\quad \div [DF^4 \sinh \{x + i(nb + \delta)\pi\} \sinh \{ \lambda_1(x + i(nb + \delta)\pi) \}]. \tag{A.2}
 \end{aligned}$$

Since $\rho_1 > \rho_2 > \rho_3$, $D < 1$. Now, for large n , from (A.2),

$$\left| \frac{F(z)}{G(z)} \right| \geq \frac{1}{D} > 1.$$

So, $|F(z)| > |G(z)|$ on the upper edge of C . In a similar manner, we can prove that $|F(z)| > |G(z)|$ on the other edges of the contour C . Hence, $|F(z)| > |G(z)|$ uniformly on the whole contour C . Therefore, by Rouché's theorem, $F(z)$ and $F(z) + G(z)$ have the same number of zeros inside the contour C , which proves that the transcendental relation (A.1) has four real roots. Hence, it is proved that the relation (3.20) has four real roots.

The investigation of the roots of $F(z) = A(z) \times B(z) = 0$ is based on the root analysis of Bhattacharjee and Sahoo [3]. Using a similar approach to that given in [3, Appendix] and with the help of Rouché's theorem, we have determined that $A(z) = 0$ has two real roots. Since the expression of $B(z)$ is similar to the expression of $A(z)$, $B(z) = 0$ also has two real roots. Hence, $F(z) = A(z) \times B(z) = 0$ has four real roots.

References

- [1] G. K. Batchelor, *An introduction to fluid dynamics* (Cambridge University Press, Cambridge, UK, 1967).
- [2] S. R. Belward and L. K. Forbes, "Fully non-linear two-layer flow over arbitrary topography", *J. Engrg. Math.* **27** (1993) 419–432; doi:10.1007/BF00128764.
- [3] J. Bhattacharjee and T. Sahoo, "Flexural gravity wave problems in two-layer fluids", *Wave Motion* **45** (2008) 133–153; doi:10.1016/j.wavemoti.2007.04.006.
- [4] J. W. Brown, R. V. Churchill and M. Lapidus, *Complex variables and applications* (McGraw-Hill, New York, 1996).
- [5] J. Candela, "Mediterranean water and global circulation", in: *Ocean circulation and climate—observing and modelling the global ocean*, Volume 77 of *Int. Geophys. Ser.* (Academic Press—Elsevier, New York, 2001), 419–429.
- [6] A. Chakrabarti and S. C. Martha, "A review on the mathematical aspects of fluid flow problems in an infinite channel with arbitrary bottom topography", *J. Appl. Math. Inform.* **29** (2011) 1583–1602; http://www.kcam.biz/contents/table_contents_view.php?Len=&idx=1281#.
- [7] M. J. Chen and L. K. Forbes, "Steady periodic waves in a threelayer fluid with shear in the middle layer", *J. Fluid Mech.* **594** (2008) 157–181; doi:10.1017/S0022112007008877.
- [8] F. Dias and J.-M. Vanden-Broeck, "Open channel flows with submerged obstructions", *J. Fluid Mech.* **206** (1989) 155–170; doi:10.1017/S0022112089002260.
- [9] F. Dias and J.-M. Vanden-Broeck, "Steady two-layer flows over an obstacle", *Philos. Trans. R. Soc. Lond. A* **360** (2002) 2137–2154; doi:10.1098/rsta.2002.1070.
- [10] F. Dias and J.-M. Vanden-Broeck, "Generalised critical free-surface flows", *J. Engrg. Math.* **42** (2002) 291–301; doi:10.1023/A:1016111415763.
- [11] L. Dongqiang, D. Shiqiang and Z. Baoshan, "Hamiltonian formulation of nonlinear water waves in a two-fluid system", *Appl. Math. Mech. (English Ed.)* **20** (1999) 343–349; doi:10.1007/BF02458559.
- [12] V. Duchêne, "On the rigid-lid approximation for two shallow layers of immiscible fluids with small density contrast", *J. Nonlinear Sci.* **24** (2014) 579–632; doi:10.1007/s00332-014-9200-2.
- [13] L. K. Forbes, "Critical free-surface flow over a semi-circular obstruction", *J. Engrg. Math.* **22** (1988) 3–13; doi:10.1007/BF00044362.
- [14] L. K. Forbes, "Two-layer critical flow over a semi-circular obstruction", *J. Engrg. Math.* **23** (1989) 325–342; doi:10.1007/BF00128906.
- [15] L. K. Forbes and G. C. Hocking, "An intrusion layer in stationary incompressible fluids. Part 2: A solitary wave", *European J. Appl. Math.* **17** (2006) 577–595; doi:10.1017/S0956792506006711.
- [16] L. K. Forbes, G. C. Hocking and D. E. Farrow, "An intrusion layer in stationary incompressible fluids. Part 1. Periodic waves", *European J. Appl. Math.* **17** (2006) 557–575; doi:10.1017/S0956792506006693.
- [17] L. K. Forbes and L. W. Schwartz, "Free-surface flow over a semicircular obstruction", *J. Fluid Mech.* **114** (1982) 299–314; doi:10.1017/S0022112082000160.
- [18] R. H. J. Grimshaw and N. Smyth, "Resonant flow of a stratified fluid over topography", *J. Fluid Mech.* **16** (1986) 429–464; doi:10.1017/S002211208600071X.
- [19] P. J. Higgins, W. W. Read and S. R. Belward, "A series-solution method for free-boundary problems arising from flow over topography", *J. Engrg. Math.* **54** (2006) 345–358; doi:10.1007/s10665-006-9039-0.

- [20] J. Kim, P. Moin and R. Moser, "Turbulence statistics in fully developed channel flow at low Reynolds number", *J. Fluid Mech.* **177** (1987) 133–166; doi:10.1017/S0022112087000892.
- [21] H. Lamb, *Hydrodynamics* (Cambridge University Press, Cambridge, 1932).
- [22] R. R. Long, "Some aspects of the flow of stratified fluids: I. A theoretical investigation", *Tellus* **5** (1953) 42–58; doi:10.1111/j.2153-3490.1953.tb01035.x.
- [23] Lord Kelvin (W. Thomson), "On stationary waves in flowing water", *Philos. Mag. Ser. 5* **22** (1886) 353–357; doi:10.1080/14786448608627944.
- [24] P. Milewski and J.-M. Vanden-Broeck, "Time dependent gravity capillary flows past an obstacle", *Wave Motion* **29** (1999) 63–79; doi:10.1016/S0165-2125(98)00021-3.
- [25] S. P. Shen, M. C. Shen and S. M. Sun, "A model equation for steady surface waves over a bump", *J. Engrg. Math.* **23** (1989) 315–323; doi:10.1007/BF00128905.
- [26] T. E. Stokes, G. C. Hocking and L. K. Forbes, "Unsteady flow induced by a withdrawal point beneath a free surface", *ANZIAM J.* **47** (2005) 185–202; doi:10.1017/S1446181100009986.
- [27] E. C. Titchmarsh, *The theory of functions*, 2nd edn (Oxford University Press, Oxford, UK, 1976).
- [28] J.-M. Vanden-Broeck, "Free-surface flow over a semi-circular obstruction in a channel", *Phys. Fluids* **30** (1987) 2315–2317; doi:10.1063/1.866121.
- [29] M. J. M. Williams, A. Jenkins and J. Determann, "Physical controls on ocean circulation beneath ice shelves revealed by numerical models", *Antarct. Res. Ser.* **75** (1998) 285–299; doi:10.1029/AR075p0285.
- [30] C. D. Winant, C. E. Dorman, C. A. Friehe and R. C. Beardsley, "The marine layer off Northern California: an example of supercritical channel flow", *J. Atmos. Sci.* **45** (1988) 3588–3605; doi:10.1175/1520-0469(1988)045<3588:TMLONC>2.0.CO;2.
- [31] Z. Yong, "Resonant flow of a fluid past a concave topography", *Appl. Math. Mech. (English Ed.)* **18** (1997) 479–482; doi:10.1007/BF02453743.